ChemComm

COMMUNICATION

View Article Online
View Journal | View Issue

Check for updates

Cite this: *Chem. Commun.*, 2025, **61**, 5015

Received 2nd January 2025,
Accepted 24th February 2025

DOI: 10.1039/d5cc00015g

rsc.li/chemcomm

Regulation of aggregation-enhanced thermally activated delayed fluorescence in butterfly-shaped donor–acceptor conjugates†

Manoj Upadhyay and Debdas Ray *

We studied how ether-linked benzophenone and dibenzofuran/dibenzothiophene-functionalized benzophenone as auxiliary groups in carbazole–phthalonitrile conjugates influence aggregation-enhanced thermally activated delayed fluorescence (AE-TADF). CDBFPN and CDBTPN exhibited AE-TADF due to their unique butterfly-shaped geometries. In contrast, CBPN faces aggregation-caused quenching, underscoring the critical role of these functionalized groups in boosting the blue TADF properties.

Organic luminescent materials that utilize both singlet and triplet excitons hold great potential for organic light-emitting diodes[1,2] and photosensitizers.[3] Yet, weak spin–orbit coupling, luminescence quenching in the aggregated state, and nonradiative decay hinder efficient triplet harnessing under ambient conditions.[4] Thermally activated delayed fluorescence (TADF) offers a solution by enabling triplet excitons to transform into radiative singlet states through reverse intersystem crossing (RISC).[1,5–7] This process relies on a small singlet–triplet energy gap (ΔE_{ST}) and orbital transformation *via* vibronic coupling. However, TADF emitters face challenges such as low RISC rates and aggregation-caused quenching (ACQ) at high doping concentrations, leading to inevitable triplet quenching due to triplet–triplet, and triplet–polaron annihilation.[8] In addition, developing blue TADF emitters is particularly difficult due to the band-gap principle.[9,10]

On the other hand, aggregation-induced emission (AIE) offers a promising solution to counteract ACQ.[9,11] AIE emitters typically feature flexible, twisted molecular structures that minimize intermolecular π···π interactions in the aggregated state, reducing emission quenching and exciton annihilation. In recent years, several TADF emitters with AIE properties have been developed, making the creation of aggregation-induced TADF enhancement emitters a desirable goal.[12–14] In the past decade, a wide variety of carbazole-based TADF emitters[6,15] were reported, but they face the ACQ effect, which limits their applications. In this work, we studied carbazole–phthalonitrile-based D–A–D conjugates, namely **CBPN**, **CDBFPN**, and **CDBTPN**, appended with benzophenone (BP) and dibenzofuran/dibenzothiophene-functionalized benzophenone (DBF-BP/DBT-BP) groups through ether linkages, resulting in twisted geometries resembling an open butterfly (Fig. 1). Through careful molecular design, we demonstrate that all these conjugates show efficient sky-blue TADF by fine-tuning the orbital nature for vibronic coupling and low energy gaps among S1, T1 and T2. Interestingly, photophysical analysis of **CDBFPN** and **CDBTPN** revealed an increase in the lifetimes of the prompt and delayed components with enhanced quantum yields (~20-fold) due to aggregation-enhanced TADF (AE-TADF) caused by the introduction of DBF/DFT units resulting in unique packing, while **CBPN** suffers from the ACQ effect. Single-crystal X-ray diffraction (SCXRD) revealed that **CDBTPN** exhibited negligible π···π interactions, unlike **CBPN**, where such interactions likely cause ACQ. This design strategy may provide valuable insights for the development of next-generation AE-TADF materials.

The final compounds were synthesized *via* two-step aromatic nucleophilic substitution reactions. All the compounds

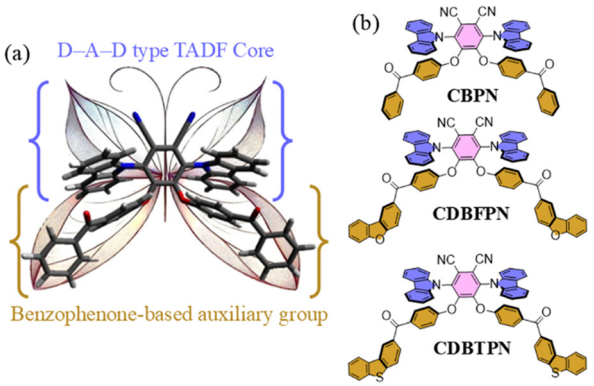

Fig. 1 (a) Molecular design and (b) structures.

Advanced Photofunctional Materials Laboratory, Department of Chemistry, Shiv Nadar Institution of Eminence, Delhi NCR, NH-91, Tehsil Dadri, Gautam Buddha Nagar, Greater Noida 201314, Uttar Pradesh, India. E-mail: debdas.ray@snu.edu.in

† Electronic supplementary information (ESI) available: Synthesis, characterization, SCXRD, electrochemical, thermal, computational analysis and PL studies provided. CCDC 2413934 and 2413935. For ESI and crystallographic data in CIF or other electronic format see DOI: https://doi.org/10.1039/d5cc00015g

Open Access Article. Published on 25 February 2025. Downloaded on 1/17/2026 1:30:53 AM.
This article is licensed under a Creative Commons Attribution-NonCommercial 3.0 Unported Licence.

Open Access Article. Published on 25 February 2025. Downloaded on 1/17/2026 1:30:53 AM.
This article is licensed under a Creative Commons Attribution-NonCommercial 3.0 Unported Licence.

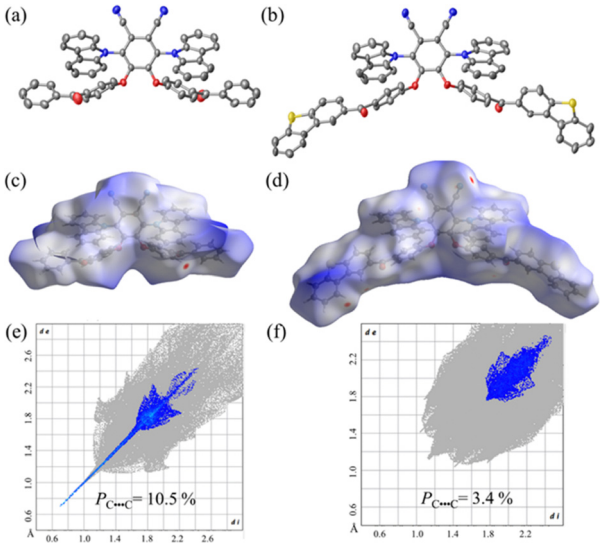

Fig. 2 Single crystal X-ray structure of (a) **CBPN** and (b) **CDBTPN**; surfaces (mapped over d_{norm}) of (c) **CBPN** and (d) **CDBTPN**; and decomposed fingerprint plots showing the proportion of intermolecular C···C interactions in (e) **CBPN** and (f) **CDBTPN**.

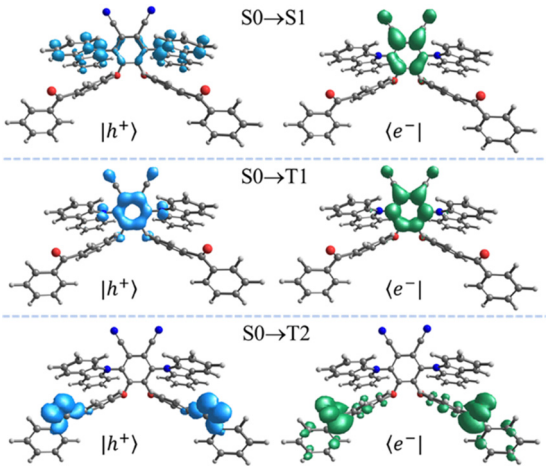

Fig. 3 Hole–electron analysis (NTOs: $|h^+\rangle$, blue; $\langle e^-|$, green) for transition orbitals corresponding to the S1, T1 and T2 excited states of **CBPN** at isosurface values of ±0.002 a.u. [M06-2X/6-31g(d,p)].

were characterized by NMR spectroscopy, high-resolution mass spectrometry, SCXRD, and HPLC analysis of the vacuum sublimated samples (ESI†).

We grew crystals of **CBPN** and **CDBTPN** using a binary solvent mixture of dichloromethane and hexane at room-temperature (RT), though **CDBFPN** failed to crystallize. SCXRD analysis revealed **CBPN** crystallizes in the centrosymmetric *C*2/*c*, while **CDBTPN** in the noncentrosymmetric *Cc* space group (Table S1, ESI†). Both adopt open, butterfly-like shapes with nearly orthogonal carbazole units, creating spatial separation of the HOMO and LUMO due to their twisted geometries (Fig. 2(a) and (b)). **CBPN** shows intermolecular π···π stacking between its carbazole fragments (3.82 Å), while **CDBTPN** lacks such interaction (Fig. S13, S14 and Table S2, ESI†). Furthermore, Hirshfeld surface analysis[16] revealed key intermolecular interactions in the crystal structures, with C–H···π interactions significantly stabilizing both molecules. **CBPN** showed stronger π···π stacking (C···C: 10.5%) than **CDBTPN** (3.4%), while **CDBTPN** had higher N···H (12.1% *vs.* 7.0%) and unique S···H (5.1%) interactions absent in **CBPN** (Fig. 2(c)–(f) and Fig. S15, Table S3, ESI†).

We analyzed the redox properties of **CBPN**, **CDBFPN**, and **CDBTPN** using cyclic voltammetry in dry DMF, referencing the ferrocene/ferrocenium (Fc/Fc^+) couple.[17] Oxidation peaks appeared at +0.69 V, +0.73 V and +0.65 V, respectively, corresponding to HOMO levels of −5.49 eV, −5.53 eV, and −5.45 eV. The LUMO levels and band gaps were −3.10 eV (**CBPN**), −3.12 eV (**CDBFPN**), and −3.09 eV (**CDBTPN**) leading to nearly similar band gaps (∼2.4 eV), indicating that all compounds possess comparable electronic structures (Fig. S16 and Table S4, ESI†). Furthermore, TGA and DSC confirmed high thermal stability, with 5% weight loss occurring at 445–460 °C and glass transition temperatures between 300–316 °C, highlighting their durability and potential for optoelectronic applications (Fig. S17 and S18, ESI†).

We used quantum chemistry calculations (DFT/TD-DFT, M06-2X/6-31G(d,p))[18] to investigate the molecule's electronic properties. Ground-state geometry optimization revealed HOMO localization on the carbazole (Cz) units and LUMO localization on the phthalonitrile (PN) segments. The BP, DBF-BP, and DBT-BP parts showed no contribution due to Cz's stronger donor strength. The minimal HOMO–LUMO overlap led to low oscillator strength and a small ΔE_{S1-T1} (Fig. S19, ESI†). The calculated vertical excitation energies aligned closely with the experimental absorption spectra, validating the reliability of the computational model (Fig. S1, ESI†). Hole–electron analysis[19] confirmed the CT character of S0 → S1 transition, driven by the H → L transition. S0 → T1 and S0 → T2 transitions revealed localized triplet state-dominated PN and keto groups, respectively (Fig. 3, Fig. S21, S22 and Table S5, ESI†). Small gaps (ΔE_{S1-T1}: 0.10–0.11 eV; ΔE_{T1-T2}: 0.2–0.21 eV) suggest efficient RISC through orbital transformation following the El-Sayed rule and vibronic coupling (Fig. S22, ESI†).

The ultraviolet-visible absorption spectra of **CBPN**, **CDBFPN**, and **CDBTPN** reveal strong bands at 300–350 nm, showing high molar absorptivity from π → π* transitions. Weaker CT bands appear at 390–450 nm, caused by donor–acceptor coupling.[7,20] A small shoulder in **CDBFPN** and **CDBTPN** at 310–340 nm can be attributed to the DBF-BP and DBT-BP segments, which are absent in **CBPN** (Fig. 4(a)). All compounds display negative solvatochromism in the lower-energy absorption bands, indicating ground state CT, and positive solvatochromism in the emission spectra, confirming CT in the excited state, which aligns with quantum chemistry calculations (Fig. 4(b) and Fig. S23, S24, ESI†). Interestingly, all three conjugates exhibit similar emission behavior in toluene (∼480 nm), indicating that CT emission predominantly originates from the Cz-PN part of the molecules (Fig. S25, ESI†). Deoxygenated conditions significantly boosted the PLQYs: 7.0% to 36.2% (**CBPN**), 6.1% to 41.5% (**CDBFPN**), and 5.2% to 45.0% (**CDBTPN**). Lifetime measurements revealed prompt and delayed components under deoxygenated conditions, which decreased with oxygen exposure, indicating triplet-state involvement (Fig. 4(c), Fig. S26 and

 This journal is © The Royal Society of Chemistry 2025

Open Access Article. Published on 25 February 2025. Downloaded on 1/17/2026 1:30:53 AM.
This article is licensed under a Creative Commons Attribution-NonCommercial 3.0 Unported Licence.

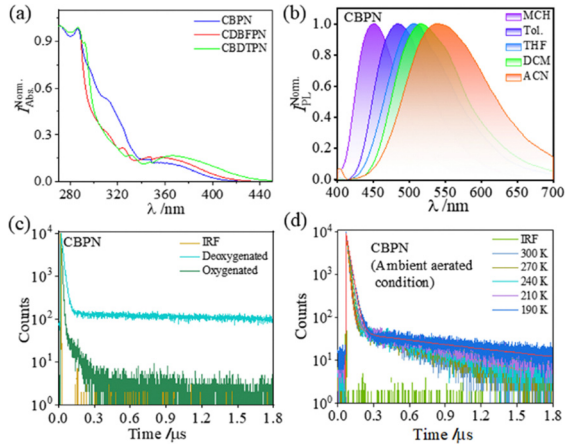

Fig. 4 (a) Absorption in toluene, and (b) solvatochromic emission of **CBPN**. (c) PL decays of **CBPN** in toluene at different conditions at RT and (d) temperature-dependent decays of **CBPN** in toluene (λ_{ex} = 370 nm; 10 μM).

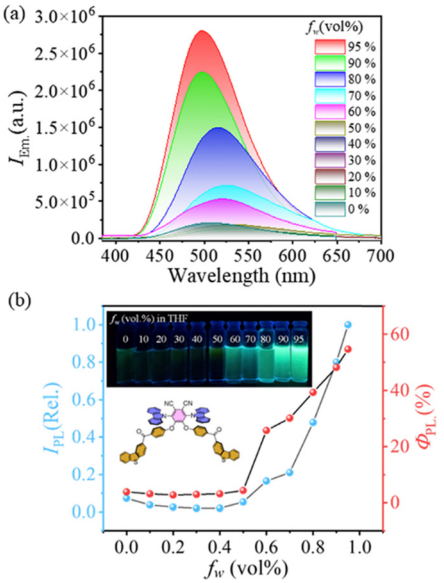

Fig. 5 (a) PL spectra of **CDBTPN** in a THF/water mixture. (b) Relative PL intensities and PLQYs of **CDBTPN** at different f_w; inset: photographs (f_w = 0% → 95%) captured under UV light.

Table S6, ESI†). Temperature-dependent fluorescence lifetime analysis under ambient aerated conditions revealed the endothermic nature of RISC (Fig. 4(d), Fig. S27 and Table S7, ESI†). Low ΔE_{ST} values at 77 K (**CBPN**: 0.17 eV, **CDBFPN**: 0.18 eV, **CDBTPN**: 0.11 eV) further validate these findings (Fig. S28, ESI†).

The aggregation effect in **CBPN**, **CDBFPN**, and **CDBTPN** was studied by increasing the water fraction (f_w) in tetrahydrofuran (THF) solutions. **CBPN** showed a decrease in emission intensity as f_w increased, indicating ACQ. In contrast, both **CDBFPN** and **CDBTPN** exhibited weak emission in THF but displayed a blue-shifted emission with significantly higher intensity and quantum yields when f_w exceeded 50%. At 95% f_w, the PLQY was 48.2% for **CDBFPN** and 54.0% for **CDBTPN**, confirming strong AIE (Fig. 5 and Fig. S29, S30, ESI†). As the solvent polarity increases, both luminogens show a bathochromic shift due to the stabilization of the CT excited states. However, at f_w = 60–95%, aggregation restricted molecular motion, inducing a hypsochromic shift. Fluorescence lifetime measurements at f_w = 95% revealed increased delayed components and lifetimes as compared to THF (**CDBFPN**: A_{DF}, 10.28 to 29.99%, τ_{DF}: 290 to 560 ns; **CDBTPN**: A_{DF}, 12.77 to 28.45%; τ_{DF}: 360 to 650 ns), supporting AE-TADF (Fig. S31 and Table S8, ESI†).[14] This effect is attributed to the aggregation of **CDBFPN** and **CDBTPN** in water, which restricts intramolecular motion and reduces nonradiative decay. The DBF-BP and DBT-BP moieties in the molecular backbone of **CDBFPN** and **CDBFPN** facilitated AE-TADF, unlike **CBPN**, which lacks these additional heteroatomic groups.[13]

Given the exceptional photophysical properties observed in solution, we systematically studied the solid-state PL properties of these molecules in both neat and doped films, using 1,3-bis(*N*-carbazolyl)benzene (mCP) as a host material at varying doping concentrations (1, 10, 20, and 30 wt%). Films were prepared by spin-coating toluene solutions of the compounds and mCP onto quartz substrates. We analyzed and compared the emission behavior of the compounds in the films. In the 1 wt% doped film, **CBPN** emitted at ~475 nm, while **CDBFPN** and **CDBTPN** emitted at ~488 nm (Fig. 6(a)). A significant bathochromic shift of 25–30 nm was observed in **CBPN** with increasing doping concentration, whereas **CDBFPN** and **CDBTPN** showed smaller shifts (12–15 nm) (Fig. S32, ESI†). This suggests that **CBPN**'s emission is more sensitive to host concentration, highlighting differences in their aggregation behaviors. As the doping concentration increased, **CBPN**'s emission became more red-shifted, indicating a concentration-dependent effect. In contrast, **CDBFPN** and **CDBTPN** displayed more stable emission behavior with minor shifts, suggesting reduced π···π interactions. The neat films showed high PLQY values of 67% and 70% for **CDBFPN** and **CDBTPN**, respectively, demonstrating resistance to ACQ. **CBPN** had a lower PLQY of 33%, attributed to strong intermolecular π···π interactions between neighbouring Cz units (Fig. 6(b)). These

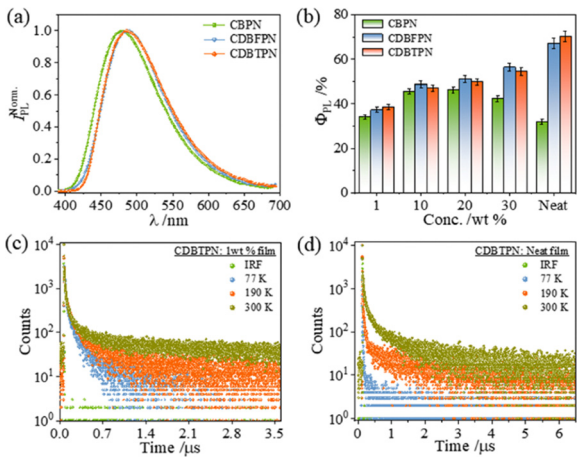

Fig. 6 (a) PL spectra of all the blend films (1 wt%). (b) PLQYs of blend samples with varying concentrations and neat films. Temperature-dependent PL decay curve of **CDBTPN**: (c) 1 wt% and (d) neat film (λ_{ex} = 370 nm).

Open Access Article. Published on 25 February 2025. Downloaded on 1/17/2026 1:30:53 AM. This article is licensed under a Creative Commons Attribution-NonCommercial 3.0 Unported Licence.

findings indicate that **CDBFPN** and **CDBTPN** exhibit robust PL performance, while **CBPN** is more susceptible to ACQ due to its molecular structure. Furthermore, fluorescence lifetime analysis of both the neat and 1 wt% doped film revealed a bi-exponential decay pattern, characteristic of both τ_{PF} and τ_{DF} (Fig. 6(c), (d) and Fig. S33, S34, ESI†). In the 1 wt% doped film, the decay times were as follows: **CBPN** (τ_{PF} = 15.6 ns, τ_{DF} = 360 ns), **CDBFPN** (τ_{PF} = 18.4 ns, τ_{DF} = 430 ns), and **CDBTPN** (τ_{PF} = 16.3 ns, τ_{DF} = 580 ns). Neat films exhibited significantly longer decay times (**CBPN:** τ_{PF} = 21.2 ns, τ_{DF} = 810 ns; **CDBFPN:** τ_{PF} = 34.9 ns, τ_{DF} = 1030 ns; **CDBTPN:** τ_{PF} = 31.4 ns, τ_{DF} = 970 ns). These extended decay times suggest stabilization of the excited states through intermolecular interactions, supporting the role of aggregation in enhancing TADF.[14] Temperature-dependent fluorescence decay analysis revealed a marked reduction in τ_{DF} with decreased contribution as the temperature decreased from 300 K to 77 K, confirming the involvement of TADF in all conjugates (Tables S9 and S10, ESI†). Additionally, we calculated k_{RISC} for both neat and doped films. The k_{RISC} values (1 wt% doped film) were 1.85×10^7 s^{-1} (**CBPN**),[7] 1.70×10^7 s^{-1} (**CDBFPN**), and 1.75×10^7 s^{-1} (**CDBTPN**). In the neat films, these values were slightly lower: 1.48×10^7 s^{-1}, 1.03×10^7 s^{-1}, and 1.27×10^7 s^{-1}, respectively. Higher k_{RISC} values in the doped film suggest faster RISC. Interestingly, the non-radiative decay rates were lower in the **CDBFPN** and **CDBTPN** neat films compared to **CBPN**, highlighting the more efficient PL behavior (Table S11, ESI†).

In summary, we synthesized three carbazole–phthalonitrile conjugates with benzophenone and its derivatives as pendent arms through ether linkages. All compounds exhibited efficient blue TADF due to small energy gaps (S1–T1, T1–T2) that favor orbital transitions. Dibenzofuran and dibenzothiophene functionalized **CDBFPN** and **CDBTPN** demonstrated aggregation-enhanced TADF, with high quantum yields. This enhancement results from reduced non-radiative decay pathways, attributed to diminished $\pi\cdots\pi$ interactions in the butterfly-like twisted geometries. Further modification of these systems and their device performance are underway.

D. R. is grateful to the Science & Engineering Research Board (SERB) (CRG/2022/000128), Department of Science and Technology (DST), India, the Anusandhan National Research Foundation (ANRF) (ANRF/IRG/2024/000038/CS) and Shiv Nadar Institution of Eminence (SNIoE). M. U. thanks SNIoE for the fellowship. The authors acknowledge the use of the high-performance computing cluster 'MAGUS' at SNIoE for providing computational resources.

Data availability

The data supporting this article have been included as part of the ESI† and can be obtained from **https://doi.org/10.1039/D5CC00015G**.

Conflicts of interest

There are no conflicts to declare.

Notes and references

1 (*a*) S. Dey, M. Hasan, A. Shukla, N. Acharya, M. Upadhyay, S.-C. Lo, E. B. Namdas and D. Ray, *J. Phys. Chem. C*, 2022, **126**, 5649–5657; (*b*) P. L. Dos Santos, J. S. Ward, D. G. Congrave, A. S. Batsanov, J. Eng, J. E. Stacey, T. J. Penfold, A. P. Monkman and M. R. Bryce, *Adv. Sci.*, 2018, **5**, 1700989.
2 H. Noda, X.-K. Chen, H. Nakanotani, T. Hosokai, M. Miyajima, N. Notsuka, Y. Kashima, J.-L. Brédas and C. Adachi, *Nat. Mater.*, 2019, **18**, 1084–1090.
3 M. A. Bryden and E. Zysman-Colman, *Chem. Soc. Rev.*, 2021, **50**, 7587–7680.
4 N. J. Turro, V. Ramamurthy and J. C. Scaiano, *Principles of molecular photochemistry: an introduction*, University Science Books, 2009.
5 (*a*) N. Acharya, M. Upadhyay, R. Deka and D. Ray, *J. Phys. Chem. C*, 2024, **128**, 8750–8758; (*b*) R. Deka, S. Dey, M. Upadhyay, S. Chawla and D. Ray, *J. Phys. Chem. A*, 2024, **128**, 581–589.
6 (*a*) I. Bhattacharjee, N. Acharya, H. Bhatia and D. Ray, *J. Phys. Chem. Lett.*, 2018, **9**, 2733–2738; (*b*) H. Uoyama, K. Goushi, K. Shizu, H. Nomura and C. Adachi, *Nature*, 2012, **492**, 234–238.
7 S. Dey, R. Deka, M. Upadhyay, S. Peethambaran and D. Ray, *J. Phys. Chem. Lett.*, 2024, **15**, 3135–3141.
8 M. A. Baldo, C. Adachi and S. R. Forrest, *Phys. Rev. B: Condens. Matter Mater. Phys.*, 2000, **62**, 10967.
9 (*a*) H. Bhatia, I. Bhattacharjee and D. Ray, *J. Phys. Chem. Lett.*, 2018, **9**, 3808–3813; (*b*) H. Bhatia and D. Ray, *J. Phys. Chem. C*, 2019, **123**, 22104–22113.
10 E. Tankelevičiūtė, I. D. Samuel and E. Zysman-Colman, *J. Phys. Chem. Lett.*, 2024, **15**, 1034–1047.
11 (*a*) H. Bhatia, S. Dey and D. Ray, *ACS Omega*, 2021, **6**, 3858–3865; (*b*) Y. Hong, J. W. Lam and B. Z. Tang, *Chem. Soc. Rev.*, 2011, **40**, 5361–5388; (*c*) S. Karmakar, S. Dey, M. Upadhyay and D. Ray, *ACS Omega*, 2022, **7**, 16827–16836; (*d*) J. Mei, N. L. Leung, R. T. Kwok, J. W. Lam and B. Z. Tang, *Chem. Rev.*, 2015, **115**, 11718–11940.
12 (*a*) H. Dai, Y. Liang, X. Long, T. Tang, H. Xie, Z. Ma, G. Li, Z. Yang, J. Zhao and Z. Chi, *Chem. Sci.*, 2025, **16**, 156–162; (*b*) Y. Matsui, Y. Yokoyama, T. Ogaki, K. Ishiharaguchi, A. Niwa, E. Ohta, M. Saigo, K. Miyata, K. Onda and H. Naito, *J. Mater. Chem. C*, 2022, **10**, 4607–4613; (*c*) F. Di Maiolo, D. A. P. Huu, D. Giavazzi, A. Landi, O. Racchi and A. Painelli, *Chem. Sci.*, 2024, **15**, 5434–5450; (*d*) Y.-Y. Hsieh, R. S. Sánchez, G. Raffy, J.-J. Shyue, L. Hirsch, A. Del Guerzo, K.-T. Wong and D. M. Bassani, *Chem. Commun.*, 2022, **58**, 1163–1166.
13 J. Guo, X. L. Li, H. Nie, W. Luo, S. Gan, S. Hu, R. Hu, A. Qin, Z. Zhao and S. J. Su, *Adv. Funct. Mater.*, 2017, **27**, 1606458.
14 W. Zhang, S. Li, Y. Gong, J. Zhang, Y. Zhou, J. Kong, H. Fu and M. Zhou, *Angew. Chem., Int. Ed.*, 2024, **63**, e202404978.
15 (*a*) D. Liu, J. Y. Wei, W. W. Tian, W. Jiang, Y. M. Sun, Z. Zhao and B. Z. Tang, *Chem. Sci.*, 2020, **11**, 7194–7203; (*b*) B. Wex and B. R. Kaafarani, *J. Mater. Chem. C*, 2017, **5**, 8622–8653.
16 P. R. Spackman, M. J. Turner, J. J. McKinnon, S. K. Wolff, D. J. Grimwood, D. Jayatilaka and M. A. Spackman, *J. Appl. Crystallogr.*, 2021, **54**, 1006–1011.
17 (*a*) C. M. Cardona, W. Li, A. E. Kaifer, D. Stockdale and G. C. Bazan, *Adv. Mater.*, 2011, **23**, 2367–2371; (*b*) N. Elgrishi, K. J. Rountree, B. D. McCarthy, E. S. Rountree, T. T. Eisenhart and J. L. Dempsey, *J. Chem. Educ.*, 2018, **95**, 197–206.
18 M. J. Frisch, *et al.*, *Gaussian 16, Revision C.01. 2016*, Gaussian Inc., Wallingford, CT, 2016.
19 T. Lu and F. Chen, *J. Comput. Chem.*, 2012, **33**, 580–592.
20 S. Dey, A. K. Pal, M. Upadhyay, A. Datta and D. Ray, *J. Phys. Chem. B*, 2023, **127**, 9833–9840.

 This journal is © The Royal Society of Chemistry 2025